

Controlling Nanometer-Scale Crystal Growth on a Model Biomaterial with a Scanning Force Microscope

R. Hariadi, S. C. Langford, and J. T. Dickinson*

Department of Physics, Washington State University, Pullman, Washington 99164-2814

Received May 23, 2002. In Final Form: August 15, 2002

We investigate the consequences of exposing an inorganic single-crystal surface to mechanical stimulation with an atomic force microscope tip in the presence of a supersaturated solution. We show that on the {010} cleavage surfaces of brushite ($\text{CaHPO}_4 \cdot 2\text{H}_2\text{O}$) layer-by-layer growth at step edges can be induced and controlled with the tip. The growth rates are highly sensitive to the crystallographic orientation of the steps. Experimental evidence is presented that supports a mechanism involving tip-enhanced mass transport of ions to nucleation sites.

Introduction

Many biological, geological, and technological processes involve crystal dissolution and growth. Growth kinetics are dominated by rates of formation of critical-sized nuclei, diffusion of components to a growing nucleus, and dissipation of the heat of crystal formation.¹ Dissolution depends on factors such as surface energetics (e.g., defects), surrounding coordination and density of solvent and various intermediate complexes, and again transport between the solvent and surface.² Thus, dissolution and growth rates are strong functions of temperature and solution chemistry as well as the composition, structure, and microtopography of the crystal surface. In particular, topographical defects (e.g., steps, kinks, and adsorbed species) are critical factors. Recent scanning force microscope (SFM) studies of calcite (CaCO_3) and brushite ($\text{CaHPO}_4 \cdot 2\text{H}_2\text{O}$) surfaces have shown that localized dissolution near the SFM probe tip can be dramatically increased by applying stress with the tip.^{3,4} In direct contrast, we show here how a SFM tip can also be used to nucleate, accelerate, and control deposition along step edges on brushite surfaces in supersaturated aqueous solutions. We present strong evidence that the tip sweeps adsorbed ions to nucleation sites by assisting them over an Ehrlich–Schwoebel type barrier parallel to the steps.^{5,6} The resulting deposition provides a unique means of generating nanometer scale structures, growing atomically flat surfaces, and new methods of controlling biomineralization. The SFM allows us to stimulate the surface with controlled scanning parameters and use the same tip to image the changes in a quantitative fashion.

Single-crystal brushite, an important biomineral and biomaterial,^{7,8} is monoclinic with space group C_s^4 or Ia . In saturated solutions, the {010} surfaces (the high stability cleavage planes) display triangular etch pits with crys-

tallographically distinct steps along the [001], [101], and [201] directions.^{9,10} These steps display three distinct bonding environments and dissolution rates. Further, the effect of high contact force scanning on the local dissolution rate varies markedly among the three steps.⁴ Calcium phosphates are important biological minerals, occurring in both normal (enamel, dentine, bone) and pathological (dental cavities, kidney stones) calcifications. Under weakly acidic conditions (pH 4–5), equilibrium conditions favor the formation of brushite. Thus the control of the growth and dissolution of phosphates have important biomedical implications.

Experimental Technique

Analytical reagent grade chemicals, distilled water, and grade A glassware are used in all experiments. Single crystals of monoclinic brushite were grown from aqueous solutions of $\text{Ca}(\text{NO}_3)_2$ and $\text{NH}_4(\text{H}_2\text{PO}_4)$ by slow diffusion in dilute nitric acid (pH 2–4) at room temperature.¹¹ In situ atomic force microscopy (AFM) imaging was performed in the contact mode with a Digital Instruments (Santa Barbara, CA) multimode scanning probe microscope at temperatures of 22–25 °C. Scanning was performed in a liquid cell with a volume of $\sim 40 \text{ mm}^3$. Commercial Si_3N_4 cantilevers with typical tip radii of $40 \pm 5 \text{ nm}$ were used in this work. Calibration of the SFM cantilever spring constant^{12–14} and the detection sensitivity for normal deflections¹⁵ were performed by standard techniques. Most of our experiments were done in supersaturated solution. The solution saturation σ is given by¹⁶

(9) Ohta, M.; Tsutsumi, M.; Ueno, S. *J. Cryst. Growth* **1979**, *47*, 135–136.

(10) Scudiero, L.; Langford, S. C.; Dickinson, J. T. *Tribol. Lett.* **1999**, *6*, 41–55.

(11) LeGeros, R. Z.; LeGeros, J. P. *J. Cryst. Growth* **1972**, *13/14*, 476–480.

(12) Hutter, J. L.; Bechhoefer, J. *Rev. Sci. Instrum.* **1993**, *64*, 1868–1873.

(13) Drexler, K. E. *Nanosystems: Molecular Machinery, Manufacturing, and Computation*; John Wiley: New York, 1992.

(14) Walters, D. A.; Cleveland, J. P.; Thomson, N. H.; Hansma, P. K.; Wendman, M. A.; Gurley, G.; Elings, V. *Rev. Sci. Instrum.* **1996**, *67*, 3583–3590.

(15) Meyer, E.; Luthi, R.; Howald, L.; Bammerlin, M. In *Micro/Nanotribology and its Applications*; Bhusan, B., Ed.; Kluwer Academic: Dordrecht, 1997; pp 193–215.

(16) Drever, J. I. *The Geochemistry of Natural Waters*, 3rd ed; Prentice Hall: Upper Saddle River, NJ, 1997.

* To whom correspondence should be addressed: jtd@wsu.edu.

(1) Chernov, A. A. *Modern Crystallography III, Crystal Growth*; Springer-Verlag: Berlin, 1984; Vol. 36.

(2) Satio, Y. *Statistical Physics of Crystal Growth*; World Scientific: Singapore, 1998.

(3) Park, N.-S.; Kim, M.-W.; Langford, S. C.; Dickinson, J. T. *J. Appl. Phys.* **1996**, *80*, 2680–2686.

(4) Scudiero, L.; Langford, S. C.; Dickinson, J. T. *Tribol. Lett.* **1999**, *6*, 41–55.

(5) Ehrlich, G.; Hudda, F. G. **1966**, *44*, 1039.

(6) Schwoebel, R. L.; Shipsey, E. J. *J. Appl. Phys.* **1966**, *37*, 3682.

(7) Siperko, L. M.; Landis, W. J. *Appl. Phys. Lett.* **1992**, *61*, 2610.

(8) Charriere, E.; Terrazzoni, S.; Pittet, C.; Mordasini, P.; Dutoit, M.; Lemaitre, J.; Zysset, P. *Biomaterials* **2001**, *22*, 2937–2945.

$$\sigma = \ln \left[\frac{a(\text{Ca}^{2+})a(\text{H}_2\text{PO}_4^-)}{K_{\text{sp}}} \right] \quad (1)$$

where $a(i)$ is the activity of the i th species and $K_{\text{sp}} = 2.57 \times 10^{-7}$ is the equilibrium solubility at zero ionic strength. Note that equilibrium is defined with respect to perfect crystals.

Results and Discussion

Figure 1 shows several etch pits in supersaturated solution. Even at these supersaturations, etch pits tend to grow (material locally dissolves) unless they are manipulated with sufficient force by the scanning probe microscope (SPM) tip. In more dilute solutions ($\sigma \sim 1$), dissolution produces etch pits with very sharp corners. However at higher supersaturations, the corner joining [201] and [101] steps becomes rounded, as shown in panels a and b of Figure 1 at $\sigma = 4$. This rounding reflects the influence of solution chemistry on the dynamics of ion removal from these two steps. Despite the fact that material is removed from the interior of the etch pits (material is dissolving), localized nucleation and growth of 3D hillocks is often observed along the top terrace edges of [201] steps, as shown in Figure 1a. Since the most favorable sites for ion attachment are actually on the lower terrace due to higher coordination, on-top nucleation indicates the presence of an Ehrlich–Schwoebel type barrier^{5,6} that hinders ion diffusion from the top terrace down to the lower terrace.

Although spontaneous pit dissolution is generally observed at these supersaturations, localized, directional growth is readily induced by continuously scanning over an etch pit at low normal forces ($F_N < 50$ nN). Growth produced by 23 scans at $F_N = 5$ nN and $\sigma = 5.3$ is shown in the sequence of images in Figure 1c, eventually filling in the pit and producing an atomically flat surface. Growth is predominately along the [201] step and propagates normal to this step. Larger images taken before and after the images in Figure 1c show that pits outside the continuously scanned area continue to dissolve even as the etch pit inside the continuously scanned area grew smaller. Thus we conclude that the observed deposition is *tip induced*. This behavior (dissolution and tip-induced growth at the same time) was observed over a wide range of supersaturations ($1 < \sigma < 6$). Scanning at $F_N > 50$ nN immediately produces localized wear (dissolution) rather than growth as previously described.¹⁰

At high saturations, growth along the [201] step induced by continuous scanning often shows a fingering instability. This is seen in the composite of two images in Figure 1b, one acquired before and one after 37 scans at $F_N = 5$ nN and a tip speed of $70 \mu\text{m/s}$. Despite this instability, continued scanning fills in the entire pit (two complete layers) and leaves no visible defects either in the topographic (constant contact force) image or in the lateral force images, although point defects such as vacancies would not be detectable in this mode of imaging.

More localized growth can be induced by drawing the SFM tip back and forth along a line normal to the [201]. Figure 2a shows a “single finger” growth feature generated by repeated linear scanning along the white line at a frequency of 2 Hz. The width of the resulting deposit is ~ 120 nm, several times wider than the region actually contacted by the tip. Assuming elastic contact, the width of the strip contacted by the moving tip is only ~ 20 nm wide. Figure 2b shows “single finger” growth formed by scanning across the [201] edge of a two atomic layer deep pit. The finger on the lower atomic layer is slightly wider

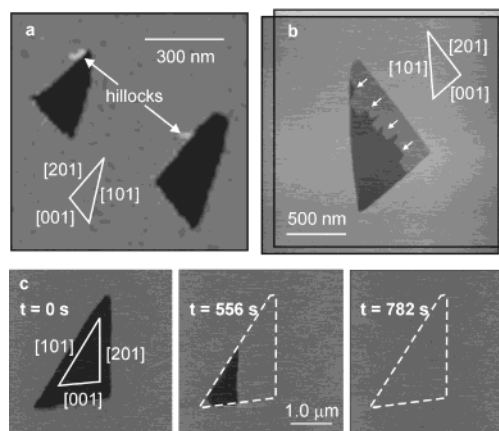


Figure 1. (a) SFM image of two spontaneously dissolving etch pits in a (010) brushite surface exposed to supersaturated solution. 3D hillock growth nucleates along the top edges of [201] steps. These hillocks are 0.8 nm high and are easily redissolved by local scanning with the SFM tip. (b) A sequence of SFM images of a one atomic layer deep etch pit in a brushite (010) surface scanned a total of 23 times at a tip speed of $70 \mu\text{m/s}$ and normal force of 5 nN. (c) Fingering growth normal to the [201] step of a single atomic layer deep etch pit during 37 scans at a normal force of 5 nN and scan speed of $70 \mu\text{m/s}$. We have superimposed images acquired before and after growth, where the darker triangle is the original pit, and new single atomic layer growth is shown in a lighter shade.

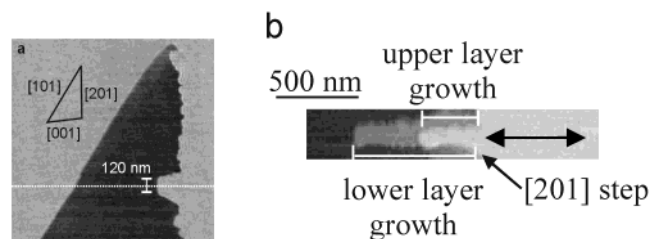


Figure 2. (a) A single atomic layer deposit ~ 120 nm wide growing normal to the [201] step produced by repeated linear scanning normal to the step. (b) Deposition in a two atomic layer deep pit showing that the lower layer grows faster than the upper layer. The arrow on the right shows the position of the linear scan over the [201] step.

and grew at approximately twice the speed of the finger on the upper layer. Growth rates vary with pit size (smaller pits shrink faster) and the degree of supersaturation, with higher σ yielding higher growth rates. At $\sigma = 5$, we have measured growth rates during linear scanning as high as 7 nm/s , corresponding to the deposition of ~ 3 rows of calcium phosphate ions per pass of the SFM tip over the step. We were unable to induce growth at [001] steps; [101] steps showed slight growth at rates $< 5\%$ of the growth rate on the [201] step.

Previous work on stress-enhanced dissolution^{3,4} indicated that the material removal rate increased continuously with increasing stress, even at very low stresses. Therefore, stress applied at or near the step edge should hinder rather than favor deposition. However, the presence of an Ehrlich–Schwoebel barrier for motion of ions down the step suggests a possible mechanism for tip-induced deposition. In supersaturated solutions, one expects the nucleation and disappearance of transient, subcritical, 3D clusters on the terraces.¹⁷ If the tip can detach and sweep ions from these clusters over the step, this would increase the concentration of adsorbed ions on the bottom terrace at the step edge and promote deposition. The

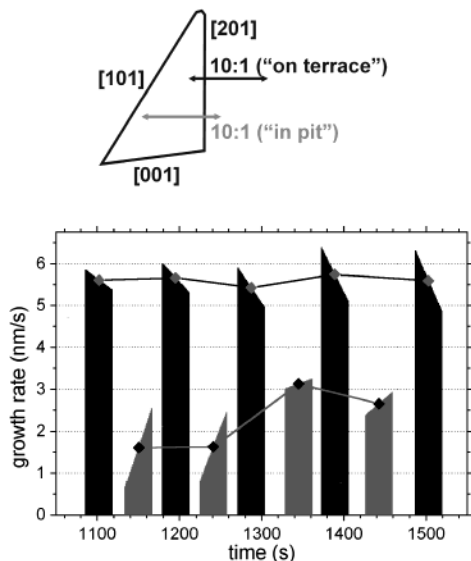


Figure 3. Comparison of growth rates along the [201] edge of a single etch pit during scanning primarily on the top terrace (10:1) (dark bars) versus primarily on the bottom terrace (1:10) (lighter bars). The top of each bar shows the growth velocity vs time during that particular set of scans. The points joined by lines join the average growth rates for each set of scans.

growth pattern in Figure 2b suggests that most of the swept material accumulates on the lower of the two terraces. Moving ions to the lowest terrace is of highest probability and would favor faster growth of the lowest finger. Diffusion along the bottom terrace would account for the broad (120 nm wide relative to the ~ 20 nm tip contact diameter) patches of deposited material in the pits near the linear scans in Figure 2. The high growth rates along the [201] steps may be due to zigzag rows of alternating Ca^{2+} and HPO_4^{2-} ions expected along these steps in order to maintain charge neutrality. This zigzag structure would provide high binding energy sites for the nucleation of new ion rows. New ion rows are much more difficult to nucleate along the other two steps.

To examine the possible role of adsorbed material swept from the upper terraces, we performed back and forth linear scans of exactly the same length ($1.5 \mu\text{m}$), normal force (10 nN), scan frequency (1.0 Hz), and number of scans (32) at the same supersaturation ($\sigma = 4.3$) but changed the fraction of the scan taking place on the top terrace. The length of the growing [201] deposit was recorded during each linear scan, and the growth rate was determined by differentiation. Figure 3 shows the measured growth rates for 10 experiments along a single [201] step, where we alternated between a 10:1 ratio of scan length on the top terrace to scan length on the bottom terrace (dark bars) and a 1:10 ratio (light bars). When the majority of the scan took place on the top terrace, the growth rates were two to three times higher than when the majority of the scan took place on the lower terrace. Very little material is swept into the pit when most of the scan is confined to the lower terrace, but scanning on the upper terrace sweeps more adsorbed material over the Ehrlich–Schwoebel barrier into the pit, where it becomes available for deposition. Note that the growth rates for the 10:1 scans consistently decrease with time (the top of each bar slopes down), consistent with the depletion of subcritical, adsorbed clusters along the upper terrace. In contrast, the growth rates for the 1:10 scans consistently increase with time (the top of each bar slopes up). This suggests that on the bottom terrace near the step, the adion concentration is initially low; as the 1:10 scans move

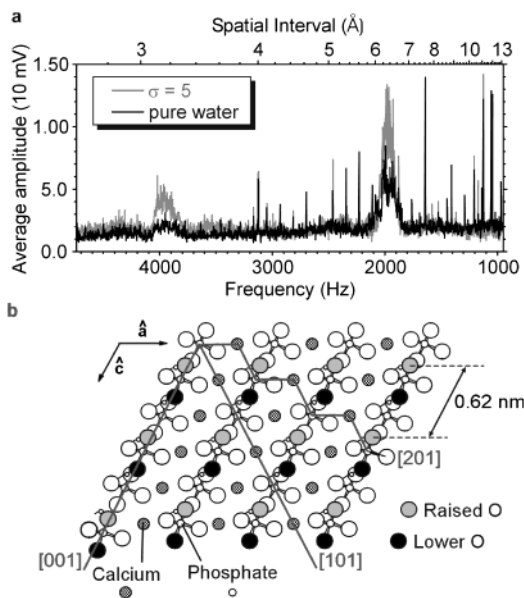


Figure 4. Characterization of fluctuations during scanning in pure water and in supersaturated solution on the (010) surface of brushite. (a) Power spectra of fluctuations in the lateral displacement of the SFM cantilever during scanning along the crystal c -axis. We attribute the higher amplitudes during scanning in supersaturated solution to increased periodic stimulation of the tip in the presence of small crystallites on the terrace. (b) Power spectra of fluctuations in the lateral displacement during scanning at 6° relative to the c -axis (perpendicular to the [201] steps). Although tip speeds were slightly different during acquisition of the data in (a) and (b), we can compare the spatial frequencies. (c) Schematic of the (010) surface of brushite.

ions into this depleted region, the growth rate increases. (A suggested and plausible ion movement mechanism was suggested by a reviewer, namely, tip-enhanced diffusion of ions to and over the step edge.)

Although transient clusters of subcritical radii were not observed in any SFM images, the fact that at high σ and long exposure times we eventually observe 3-D nucleation on atomically flat terraces and away from step edges strongly supports their existence. We have acquired indirect evidence for their presence by examining small fluctuations (“noise”) in the lateral twist of the SFM cantilever.¹⁸ (The lateral twist of the cantilever is highly sensitive to surface roughness.) These fluctuations are much stronger during scanning in highly supersaturated solution ($\sigma = 5$) than during scanning in pure water (no cluster formation). Figure 4a shows power spectra of the fluctuations averaged over 10 $1\text{-}\mu\text{m}$ linear scans along the crystal’s c -axis at $1.25 \mu\text{m/s}$ and $F_N = 5$ nN in supersaturated solution and in pure water. Both power spectra in Figure 4a show peaks near ~ 2 and 4 kHz, but their amplitudes in supersaturated solution are higher by a factor of 2. The spatial frequency corresponding to the larger 2 kHz peak (given by the scan speed/frequency) is 0.63 nm. This corresponds well with the distance between the uppermost phosphate oxygen ions (which interact most strongly with tip asperities) along the c -axis of the unreconstructed (010) surface of 0.62 nm.^{19,20} A schematic of an unrelaxed brushite cleavage plane (010) is shown in Figure 4b. We propose that this peak is due to a periodic

(18) Hariadi, R.; Dickinson, J. T. In preparation.

(19) Wyckoff, R. W. G. *Crystal Structures*, 2nd ed; Interscience: New York, 1965; Vol. 3.

(20) Curry, N. A.; Jones, S. W. *J. Chem. Soc. A* **1971**, 1971, 3725–3729.

rocking motion induced in the tip as asperities interact collectively with successive rows of oxygen ions. The second harmonic arises due to a nonlinearity in the cantilever response.

A related mechanism accounts for many images showing atomic-scale periodic structures (not true atomic resolution) with relatively large radii SFM tips acquired in contact mode on graphite,²¹ brushite,⁴ calcite (another crystal with protruding oxygen ions),^{22–24} and other single crystals. The resonant frequency of the lateral twist of our cantilevers (estimated from the properties of Si₃N₄ and the dimensions of our cantilevers) is ~40 kHz, high above the observed spectral features. We propose that the increased amplitude of cantilever rocking at high saturations is caused by tip–cluster collisions and therefore serves as evidence of transient clusters on the terraces. These collisions may increase normal mode motion which enhances the lateral deflection due to stronger interactions with the lattice. Numerous noise measurements in both pure water and saturated solutions at various scanning directions all show comparable increases in amplitude for the saturated solutions supporting our hypothesis. Similarly, scanning atomically flat brushite terraces vs regions with high densities of single atomic layer steps

(21) Ruan, J.-A.; Bhushan, B. *J. Appl. Phys.* **1994**, *76*, 5022–5035.

(22) Ohnesorge, F.; Binnig, G. *Science* **1993**, *260*, 1451–1456.

(23) Hillner, P. E.; Manne, S.; Gratz, A. J.; Hansma, P. K. *Ultra-microscopy* **1992**, *42–44*, 1387–1393.

(24) Liang, Y.; Lea, A. S.; Baer, D. R.; Engelhard, M. H. *Surf. Sci.* **1996**, *351*, 172–182.

show precisely the same response: an increase in noise amplitude for the latter surfaces.

4. Conclusion

We have shown that low normal force scanning of the surface of an ionic crystal (brushite) with an SFM tip in supersaturated solution can induce and control deposition and atomic layer regrowth at step edges. This process can be exploited to produce atomically smooth surfaces by “filling” rather than “polishing”. The chief role of the tip appears to be the controlled transport of sorbed ion clusters from upper terraces over the step edge, thereby raising concentration of adsorbed ions near the step inside the pit. Second, 3D nucleation is totally suppressed by scanning, thereby maintaining flat surfaces. The use of fluctuations (“noise”) in the lateral rocking of the cantilever to probe dynamic processes during deposition, such as the formation of transient sorbed clusters, is an exciting prospect. Ongoing studies include manipulation of both layered and 3D growth to produce novel nanometer dimension structures on surfaces of inorganic single-crystal materials.

Acknowledgment. We thank Louis Scudiero for his assistance in the laboratory and John Hirth for helpful discussions. This work was supported by the National Science Foundation under Grant CMS-01-16196 and a subcontract with the University of Florida on a KDI-NSF Collaboration, Grant No. 9980015.

LA025984F